A Density Functional Theory for Lennard-Jones Fluids in Cylindrical Pores and Its Applications to Adsorption of Nitrogen on MCM-41 Materials

Bo Peng and Yang-Xin Yu*

Department of Chemical Engineering, Tsinghua University, Beijing 100084, People's Republic of China, and State Key Laboratory of Chemical Engineering, Tsinghua University, Beijing 100084, People's Republic of China

Received July 29, 2008. Revised Manuscript Received September 5, 2008

A density functional theory (DFT) constructed from the modified fundamental-measure theory and the modified Benedict−Webb−Rubin equation of state is presented. The Helmholtz free energy functional due to attractive interaction is expressed as a functional of attractive weighted-density in which the weight function is a mean-field-like type. An obvious advantage of the present theory is that it reproduces accurate bulk properties such as chemical potential, bulk pressure, vapor−liquid interfacial tension, and so forth when compared with molecular simulations and experiments with the same set of molecular parameters. Capabilities of the present DFT are demonstrated by its applicability to adsorption of argon and nitrogen on, respectively, a model cylindrical pore and mesoporous MCM-41 materials. Comparison of the theoretical results of argon in the model cylindrical pore with those from the newly published molecular simulations indicates that the present DFT predicts accurate average densities in the pore, slightly overestimates the pore pressure, and correctly describes the effect of the fluid−pore wall interaction on average densities and pressures in the pore. Application to adsorption of nitrogen on MCM-41 at 77.4 K shows that the present DFT predicts density profiles and adsorption isotherms in good agreement with those from molecular simulations and experiments. In contrast, the hysteresis loop of adsorption calculated from the mean-field theory shifts toward the low pressure region because a low bulk saturated pressure is produced from the mean-field equation of state. The present DFT offers a good way to describe the adsorption isotherms of porous materials as a function of temperature and pressure.

1. Introduction

Fluids adsorbed in meso- and microporous materials exhibit a wide range of phase behavior that is very different from and even much richer than that of the corresponding bulk state.[1] These interesting surface-driven phase behaviors steming from the introduction of confinement have widely practical applications such as gas storage,[2,3] chromatography, oil recovery, and membrane technologies.[4] As the need for a deep understanding of newly synthesized materials such as carbon nanotubes and molecular sieves increases, a wide range of theoretical and molecular simulation research works have been carried out to help understand and explain experiment results.[5−9] Instead of classical thermodynamics, statistical mechanic theories are used to predict fluids confined in narrow pores because of the highly inhomogeneous nature of the confined fluid.[10] Density functional theory (DFT), which is based on the idea that the free energy of the inhomogeneous fluid can be expressed as a functional of spatial variation of the average one-body density $\rho(r)$,[11] has proved to be a very successful and general method for analyzing the thermodynamic and structural properties of inhomogeneous fluids.[12]

In the past years, a combination of the mean-field (MF) approximation on different versions of DFTs has been used to elucidate the phase diagrams of simple fluids in narrow pores. It has proved that the crudest local density approximation (LDA) gives a poor representation of the fluid structure and fails to reproduce the phase diagrams and adsorption isotherm, while Tarazona's smoothed density approximation (SDA)[13,14] provides a quite accurate result in good agreement with the simulation data.[10] In the SDA of Tarazona, smoothed density is weight averaged over the original density profile with weighting functions chosen to fit the direct correlation functions of the bulk fluids. In contrast to most alternative DFTs, the fundamental measure theory (FMT) of Rosenfeld[15] and its variations[16−18] do not require the direct correlation function as an input, but rather reproduce the Percus−Yevick direct correlation function as an output in the limit of bulk fluid. They represent a special position for their appealing theoretical background and high accuracy for a wide class of models for which a shape of particle is well defined. In particular, the modified fundamental measure theory (MFMT) proposed by Yu et al.[16,17] predicts very accurate density profiles and adsorption isotherms for hard spheres and polydisperse hard-sphere mixtures inside slitlike and cylindrical pores,[3] around

* Corresponding author. E-mail: yangxyu@mail.tsinghua.edu.cn.

(1) Gelb, L. D.; Gubbins, K. E.; Radhakrishnan, R.; Sliwinska-Bartkoviak, M. *Rep. Prog. Phys.* **1999**, *62*, 1573–1659.
(2) Rosi, N. L.; Eckert, J.; Eddaoudi, M.; Vodak, D. F.; Kim, J.; O'Keefe, M.; Yaghi, O. *Science* **2003**, *300*, 1127–1129.
(3) Gu, C.; Gao, G.-H.; Yu, Y.-X. *J. Chem. Phys.* **2003**, *119*, 488–495.
(4) Magda, J. J.; Tirrell, M.; Davis, H. T. *J. Chem. Phys.* **1985**, *83*, 1888–1901.
(5) Zhu, J.; Wang, Y.; Li, W. J.; Wei, F.; Yu, Y.-X. *Nanotechnology* **2007**, *18*, 095707.
(6) Ravikovitch, P. I.; Neimark, A. V. *Langmuir* **2006**, *22*, 11171–11179.
(7) Nguyen, T. X.; Bhatia, S. K.; Nicholson, D. *Langmuir* **2005**, *21*, 3187–3197.
(8) Bhatia, S. K.; Myers, A. L. *Langmuir* **2006**, *22*, 1688–1700.
(9) Koga, K.; Tanaka, H.; Zeng, X. Z. *Nature* **2000**, *408*, 564–567.
(10) Bratko, D.; Blum, L.; Wertheim, M. S. *J. Chem. Phys.* **1989**, *90*, 2752–2757.
(11) Evans, R., In *Fundamentals of Inhomogeneous Fluids*; Henderson, H., Ed.; Dekker : New York, 1992; Chapter 3, p 85.
(12) Balbuena, P. B.; Gubbins, K. E. *Langmuir* **1993**, *9*, 1801–1814.
(13) Tarazona, P. *Phys. Rev. A* **1985**, *31*, 2672–2679.
(14) Tarazona, P. *Phys. Rev. A* **1985**, *32*, 3148–3148.
(15) Rosenfeld, Y. *Phys. Rev. Lett.* **1989**, *63*, 980–903.
(16) Yu, Y.-X.; Wu, J. Z. *J. Chem. Phys.* **2002**, *117*, 10156–10164.
(17) Yu, Y.-X.; Wu, J. Z.; Xin, Y.-X.; Gao, G.-H. *J. Chem. Phys.* **2004**, *121*, 1535–1541.
(18) Tarazona, P. *Phys. Rev. Lett.* **2000**, *84*, 694–697.

10.1021/la8024099 CCC: $40.75
Published on Web 10/08/2008

cylinders,[19] and around spherical solid surfaces as well as the correlation functions for homogeneous hard spheres and polydiperse hard-sphere mixtures. For a hard-sphere fluid near a soft wall, Ravikovitch et al.[20] showed that both the SDA and FMT predicted density profiles in good agreement with that of grand canonical ensemble Monte Carlo (GCMC) simulations.

However, in most applications of DFT to gas adsorptions,[7,20−22] the MF theory was used to implement the attractive contribution to the Helmholtz free energy functional. The main discrepancies between the MF approximation DFT and molecular simulations lie in the bulk properties, which are determined by the attractive MF part in the DFT. The MF theory fails to reproduce the phase diagram of molecular simulations and experiments with the same set of molecular parameters because of the neglect of the attractive forces on the intermolecular correlations. This is very obvious at low pressure, especially when capillary condensation is concerned. As a result, the different sets of parameters have to be determined from the fit of the DFT equation of state to experimental data at a specific temperature.[7,20−22] A number of attempts have been made to obtain an improved description of the attractive interactions. Medros et al.[23] proposed a perturbation weighted density approximation for the contribution of the attractive interaction with a local compressibility equation, which gives a good description of a bulk phase diagram of Lennard-Jones fluid as simulations. In recent years, researchers[24−26] tried to evaluate the attractive contribution to the Helmholtz free energy functional through a quadratic functional Taylor expansion around a uniform fluid, and have achieved great successes. In these approaches, the direct correlation function of the bulk fluid was used as an input, and the hard-core contribution was obtained from the MFMT. To our knowledge, there is no report on the application of the DFT to the fluid confined in a cylindrical pore in which the used DFT could reproduce the accurate bulk properties of the molecular simulations and experiments.

The main goal of this work is to make a step toward using DFT to reproduce the results of molecular simulations and experiments. We present a DFT based on the MFMT and the modified Benedict−Webb−Rubin (MBWR) equation of state.[27] In order to correct the deviation of the MF approximation DFT to molecular simulations, the MBWR equation of state and a weighted density of attractive interaction evaluated in an MF way are selected to reduce the deviations between the theory and experiments in the bulk case. In this way, the DFT could give a good description of the Helmholtz energy for both inhomogeneous and homogeneous fluid, which is comparable to the molecular simulation results. We will test the proposed method by applying it to the adsorption and desorption in the cylindrical confinement in this work.

The rest of this paper is organized as follows. In section 2 we briefly describe the DFT proposed in this paper. Numerical results for the bulk surface tension, density profiles, and adsorption isotherms are presented and compared with molecular simulations and experiments in section 3. The proposed DFT will be tested against molecular simulation data of argon adsorption in model cylindrical pores, and applications to nitrogen adsorption on MCM-41 will be presented in this section. Some conclusions are given in section 4.

2. Density Functional Theory

In a DFT, the grand potential functional $\Omega[\rho(\mathbf{r})]$ of the system can be expressed as a functional of one-body fluid density distribution of fluid through the Legendre transform:

$$\Omega[\rho(\mathbf{r})] = F[\rho(\mathbf{r})] + \int [V^{\text{ext}}(\mathbf{r}) - \mu]\rho(\mathbf{r})\mathrm{d}\mathbf{r} \tag{1}$$

where $F[\rho(\mathbf{r})]$ is the intrinsic Helmholtz energy functional, $V^{\text{ext}}(\mathbf{r})$ represents the external potential exerted by the pore wall, μ is the chemical potential, and $\rho(\mathbf{r})$ is the one-body fluid density distribution. In equilibrium, the density distribution corresponding to the minimum of the grand potential is obtained from the Euler equation:

$$\left(\frac{\delta\Omega[\rho(\mathbf{r})]}{\delta\rho(\mathbf{r})}\right)_{\mu,V,T} = 0 \tag{2}$$

The Helmholtz free energy functional can be expressed as a sum of an ideal gas plus an excess term:

$$F[\rho(\mathbf{r})] = F^{\text{id}}[\rho(\mathbf{r})] + F^{\text{ex}}[\rho(\mathbf{r})] \tag{3}$$

The ideal gas term is known exactly from classical statistical mechanics:

$$F^{\text{id}}[\rho(\mathbf{r})] = k_{\text{B}}T\int \rho(\mathbf{r})\{\ln[\rho(\mathbf{r})\Lambda^3] - 1\}\mathrm{d}\mathbf{r} \tag{4}$$

where $\Lambda = (h^2/2\pi m k_{\text{B}}T)^{1/2}$ is the thermal de Broglie wavelength, h is the Planck constant, m is the mass of the fluid molecule, k_{B} is the Boltzmann constant, and T is the absolute temperature. The excess free energy functional can be decomposed into the contribution from hard-core repulsion, and that due to long-range attractive interactions:

$$F^{\text{ex}}[\rho(\mathbf{r})] = F^{\text{ex}}_{\text{hs}}[\rho(\mathbf{r})] + F^{\text{ex}}_{\text{att}}[\rho(\mathbf{r})] \tag{5}$$

where the subscripts hs and att represent, respectively, the hard-sphere and attractive contributions to the Helmholtz free energy functional. If we use Lennard-Jones potential to represent the interactions between fluid molecules, the separation of fluid−fluid intermolecular potential can be made on the basis of the weighted curvature approximation scheme[28]

$$u_{\text{att}}(r) = \begin{cases} -\varepsilon & r < r_{\text{m}} \\ 4\varepsilon\left[\left(\frac{\sigma}{r}\right)^{12} - \left(\frac{\sigma}{r}\right)^{6}\right] & r_{\text{m}} < r < r_{\text{c}} \\ 0 & r < r_{\text{c}} \end{cases} \tag{6}$$

where σ and ε are, respectively, the well depth and distance parameters of the Lennard-Jones potential, r_{m} is the distance where the intermolecular potential reaches a minimum, i.e., $r_{\text{m}} = 2^{1/6}\sigma$, and r_{c} is the cutoff distance.

To derive the excess Helmholtz energy functional due to hard sphere, we follow the procedure proposed by Yu and Wu:[16,17]

$$F^{\text{ex}}_{\text{hs}}[\rho(\mathbf{r})] = k_{\text{B}}T\int \Phi^{\text{hs}}[n_\alpha(\mathbf{r})]\mathrm{d}\mathbf{r} \tag{7}$$

where $\Phi^{\text{hs}}[n_\alpha(\mathbf{r})]$ is the excess Helmholtz free-energy density due to the hard-core repulsion, and $n_\alpha(\mathbf{r})$ is the hard-sphere weighted density defined as

(19) Wang, K.; Yu, Y.-X.; Gao, G.-H. *J. Chem. Phys.* **2008**, *128*, 185101.
(20) Ravikovitch, P. I.; Vishnyakov, A.; Neimark, A. V. *Phys. Rev. E* **2001**, *64*, 011602.
(21) Ustinov, E. A.; Do, D. D. *Langmuir* **2003**, *19*, 8349–8357.
(22) Ustinov, E. A.; Do, D. D.; Jaroniec, M. *Appl. Surf. Sci.* **2005**, *252*, 548–561.
(23) Mederos, L.; Navascues, G.; Tarazona, P.; Chacon, E. *Phys. Rev. E* **1993**, *47*, 4284–4288.
(24) Yu, Y.-X.; You, F.-Q.; Tang, Y.; Gao, G.-H.; Li, Y.-G. *J. Phys. Chem. B* **2006**, *110*, 334–341.
(25) You, F.-Q.; Yu, Y.-X.; Gao, G.-H. *J. Phys. Chem. B* **2005**, *109*, 3512–3518.
(26) Kim, S. C.; Lee, S. H. *J. Phys.: Condens. Matter* **2004**, *16*, 6365–6374.
(27) Johnson, J. K.; Zollweg, J. A.; Gubbins, K. E. *Mol. Phys.* **1993**, *78*, 591–618.
(28) Weeks, J. D.; Chandler, D.; Andersen, H. C. *J. Chem. Phys.* **1971**, *54*, 5237–5247.

$$n_\alpha(\mathbf{r}) = \int d\mathbf{r}'\rho(\mathbf{r}')w^{(\alpha)}(\mathbf{r}-\mathbf{r}') \quad (8)$$

where $\alpha = 1, 2, 3, V1$, and V2. The weight functions $w^{(\alpha)}(\mathbf{r})$ are given by[15]

$$w^{(2)}(\mathbf{r}) = \pi d^2 w^{(0)}(\mathbf{r}) = 2\pi d w^{(1)}(\mathbf{r}) = \delta(d/2 - r) \quad (9)$$

$$w^{(3)}(\mathbf{r}) = \Theta(d/2 - r) \quad (10)$$

$$w^{(V2)}(\mathbf{r}) = 2\pi d w^{(V1)}(\mathbf{r}) = \frac{\mathbf{r}}{r}\delta(d/2 - r) \quad (11)$$

where $\Theta(r)$ is the Heaviside step function, d is the effective hard-sphere diameter, and $\delta(r)$ denotes the Dirac delta function. In the MFMT, the Helmholtz free-energy density consists of terms dependent on scalar- and vector-weighted densities:

$$\Phi^{hs}[n_\alpha(r)] = \Phi^{hs(S)}[n_\alpha(r)] + \Phi^{hs(V)}[n_\alpha(r)] \quad (12)$$

where the superscripts (S) and (V) represent the contributions from scalar- and vector-weighted densities, respectively. The scalar Helmholtz energy density is given by[16,17]

$$\Phi^{hs(S)}[n_\alpha(r)] = -n_0\ln(1-n_3) + \frac{n_1 n_2}{1-n_3} + \frac{n_2^3\ln(1-n_3)}{36\pi n_3^2} + \frac{n_2^3}{36\pi n_3(1-n_3)^2} \quad (13)$$

and the vector part is expressed by

$$\Phi^{hs(V)}[n_\alpha(r)] = -\frac{\mathbf{n}_{V1}\cdot\mathbf{n}_{V2}}{1-n_3} - \frac{n_2\mathbf{n}_{V2}\cdot\mathbf{n}_{V2}\ln(1-n_3)}{12\pi n_3^2} - \frac{n_2\mathbf{n}_{V2}\cdot\mathbf{n}_{V2}}{12\pi n_3(1-n_3)^2} \quad (14)$$

In the limit of the homogeneous fluid, the two vector-weighted densities $\mathbf{n}_{V1}$ and $\mathbf{n}_{V2}$ vanish, and the Helmholtz free-energy density becomes identical to that derived from the Carnahan−Starling equation of state.[29]

To obtain the contribution of long-range van der Waals interaction to the excess Helmholtz energy functional, the MF theory was traditionally used. In the MF theory, the attractive contribution is expressed as

$$F^{att}[\rho(r)] = \frac{1}{2}\int\int\rho(\mathbf{r})\rho(\mathbf{r}')u^{att}(|\mathbf{r}-\mathbf{r}'|)d\mathbf{r}d\mathbf{r}' \quad (15)$$

The bulk chemical potential and pressure of the fluid is described by the following equation of state:

$$\mu(\rho) = \mu_{hs}(\rho) + \rho\int u_{att}(r)d\mathbf{r} \quad (16)$$

$$p = p_{hs} + \frac{1}{2}\rho^2\int u_{att}(r)d\mathbf{r} \quad (17)$$

where $\mu_{hs}(\rho)$ and p_{hs} are the chemical potential and the pressure of the hard-sphere fluid, respectively. Regrettably, eqs 16 and 17 are unable to accurately describe the bulk properties of the fluid. Thus, in this work we use a mean-field weighted density functional theory (MFWDFT) for the attractive contribution to the excess Helmholtz free energy functional, which is expressed as

$$F^{att}[\rho(\mathbf{r})] = \int\overline{\rho}(\mathbf{r})\psi^{att}[\overline{\rho}(\mathbf{r})]d\mathbf{r} \quad (18)$$

where $\psi^{att}[\overline{\rho}(\mathbf{r})]$ is the attractive contribution to the excess Helmholtz free energy per particle of a bulk fluid with density $\overline{\rho}(\mathbf{r})$. The weighted density for attractive part, $\overline{\rho}(\mathbf{r})$, is defined by

$$\overline{\rho}(\mathbf{r}) = \int\rho(\mathbf{r}')w^{(att)}(|\mathbf{r}-\mathbf{r}'|)d\mathbf{r}' \quad (19)$$

where $w^{(att)}(r)$ is a normalized weight function, and in the MF theory it can be obtained by

$$w^{(att)}(r) = u^{att}(r)/\int u^{att}(r)d\mathbf{r} \quad (20)$$

In order to obtain accurate bulk properties for the Lennard-Jones fluid, we adopt the MBWR equation of state with the parameters given by Johnson et al.[27] In the MBWR equation of state,[27] the attractive contribution to the excess Helmholtz free energy per particle takes the form

$$\psi^{att}(\rho) = \varepsilon\sum_{i=1}^{8}\frac{a_i(\rho^*)^i}{i} + \varepsilon\sum_{i=1}^{6}b_iG_i - \psi^{CS} \quad (21)$$

where the coefficients a_i and b_i are functions of temperature only, and the coefficients G_i are functions of density. The functional forms of the a_i, b_i, and G_i as well as the values of the parameters for the MBWR equation of state[27] can be found in ref 27. ψ^{CS} is the hard-sphere part of the Helmholtz free energy per particle obtained from the Carnahan−Starling equation of state:[29]

$$\psi^{CS}(\rho) = k_BT\frac{4\eta - 3\eta^2}{(1-\eta)^2} \quad (22)$$

where $\eta = \pi\rho d^3/6$ is the packing fraction.

Once we have the expression of excess Helmholtz free energy functional, we can use the Euler equation to obtain the equilibrium density profiles by an iteration method. In all the following results, the reduced quantities are used. For example, reduced density $\rho^* = \rho\sigma^3$, reduced temperature $T^* = k_BT/\varepsilon$, reduced pore diameter $D^* = D/\sigma$, reduced pressure $p^* = p\sigma^3/\varepsilon$, and reduced chemical potential $\mu^* = \mu/\varepsilon$.

3. Results and Discussion

3.1. Phase Equilibrium and Surface Tension of Bulk Fluid. A good DFT should not only predict the accurate density profile in confining geometry, but also reproduce the thermodynamic properties of bulk fluid. The bulk phase diagram of the Lennard-Jones fluid predicted from the MF and MBWR[27] equations of state are compared with molecular simulation data[30,31] in Figure 1. The MBWR equation of state gives a very good description of the bulk phase behavior of the Lennard-Jones fluid when compared with the molecular simulations. Since the results of the MF theory are dependent on the hard sphere diameter used, the MF theory may lead to excellent agreement with molecular data if the expression of hard-sphere diameter is properly chosen.[32] Two cases, i.e., the hard-sphere diameter of Lu et al.[33] and of $d = \sigma$ are considered in Figure 1a. The MF theory fails to give a good description of bulk properties, especially in saturated liquid density and pressure, just as concluded by Gubbins.[34] Although the prediction of saturated liquid density may be

(29) Carnahan, N. F.; Starling, K. E. *J. Chem. Phys.* **1969**, *51*, 635–636.
(30) Lotfi, A.; Vravec, J.; Fischer, J. *Mol. Phys.* **1992**, *76*, 1319–1333.
(31) Hamada, Y.; Koga, K.; Tanaka, H. *J. Chem. Phys.* **2007**, *127*, 084908.
(32) Figueroa-Gerstenmaier, S. *J. Chem. Phys.* **2003**, *118*, 830–841.
(33) Lu, B. Q.; Evans, R.; Da Gama, M. M. T. *Mol. Phys.* **1985**, *55*, 1319–1338.
(34) Gubbins, K. E. *Phys. Adsorpt.: Exp., Theory Appl.* **1997**, *65*, 103.

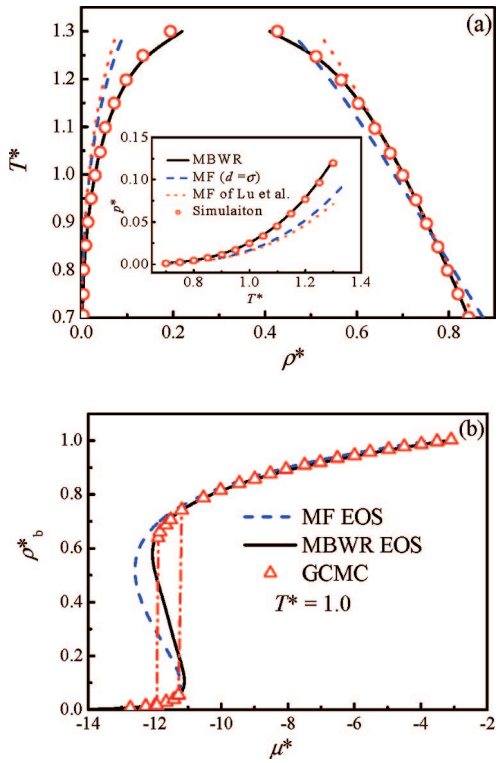

Figure 1. (a) Vapor−liquid phase diagram and saturated vapor pressure (inset) of the Lennard-Jones fluid with cutoff distance $r_c = 5\sigma$ and (b) $\rho^*-\mu^*$ isotherms of the Lennard-Jones fluid. Solid, dashed, and dotted lines represent the results from the MBWR equation of Johnson et al.,[27] MF equation of state with hard-sphere diameter $d = \sigma$, and with the diameter from Lu et al.,[33] respectively. Opened circles and triangles represent the molecular simulation data of Lotfi et al.[30] and Hamada et al.,[31] respectively. Dash−dotted lines in panel b indicate hysteresis loop from the molecular simulations.

improved using the diameter by Lu et al.,[33] the deviations between calculated pressure and the simulation pressure are larger than those from MF theory with $d = \sigma$. In general, the MF theory overestimates the critical temperature of the Lennard-Jones fluid. Figure 1b shows that MF theory with hard-sphere $d = \sigma$ gives a good description at low density and high density in the density−chemical potential plane at reduced temperature $T^* = 1.0$. It should be pointed out that Ravikovitch and Neimark[20] tested different versions of the MF theory by varying potential splitting methods and hard-sphere diameter, and found that none of the MF theories can reproduced both equilibrium liquid density and saturated pressure in the full range of temperature. Then they fitted the MF equation of state to experimental data to obtain the Lennard-Jones parameters for the MF theory. In their method, two sets of different Lennard-Jones parameters are used for molecular simulation and nonlocal DFT calculations. Because our DFT is based on the MBWR equation of state, which reproduces the bulk properties very well, it is possible for us to use the same set of Lennard-Jones parameters for both simulations and DFT calculations. Furthermore we select a hard-sphere diameter $d = \sigma$ in both the MF theory and DFT calculations in this paper.

An accurate prediction of surface tension of bulk fluid is the first step for a model to describe vapor−liquid phase transition in pores. Thus the surface tensions of argon and nitrogen are predicted from the present DFT and the results are compared with those from molecular simulation,[35] experiments,[36,37] and

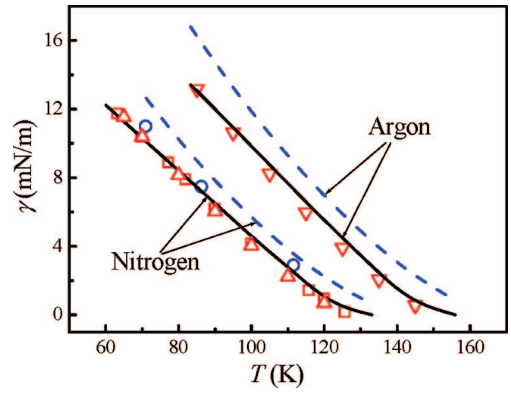

Figure 2. Comparison of the predicted vapor−liquid surface tensions with the experimental data and simulation results for argon and nitrogen. Open circles, solid lines, and dashed lines represent the results from the molecular dynamics simulations,[35] present DFT theory, and MF theory, respectively. Open squares represent the experimental data of nitrogen from Yaws.[36] Up- and down-triangles represent the experimental data from Kai et al.[37] for nitrogen and argon, respectively. In the theoretical calculation, a cut-and-shifted distance $r_c = 5\sigma$ was used.

MF theory in Figure 2. In both the MF theory and present DFT, the surface tension of the vapor−liquid interface was obtained from the excess grand potential of the system by

$$\gamma = (\Omega - \Omega^b)/A \tag{23}$$

where A is the area of the interface, and Ω and Ω^b are the grand potentials containing two phases in equilibrium and one bulk phase (saturated vapor or liquid), respectively. In the theoretical calculations, the Lennard-Jones parameters for argon and nitrogen are the same as used in the molecular simulations, i.e., $\sigma = 0.340$ nm and $\varepsilon/k_B = 119.0$ K for argon[7] and $\sigma = 0.3615$ nm and $\varepsilon/k_B = 101.5$ K for nitrogen.[20] The experimental surface tensions of argon and nitrogen were obtained from the empirical formula of Kai et al.[37] with the critical temperatures from Reid et al.[38] It can bee seen from Figure 2 that the present DFT predicts the surface tensions for both argon and nitrogen in good agreement with the simulation and experimental data, while the MF theory overestimates the surface tensions in the whole temperature range considered.

3.2. Lennard-Jones Fluid Adsorption in Model Cylindrical Pores. Lennard-Jones potential is a good model for argon and nitrogen, as shown in the previous section. The cylindrical pore is a more closed system compared to a slit pore. In our experience with cylindrical pores with a radii smaller than 5σ, we have found that it takes fairly a long time for the molecules to move to a compact structure because of the large curvature of the small pore. It is interesting to note that, compared to the previous work,[39] recent molecular simulations[40] begin to realize this problem, and more additional configurations are calculated using powerful supercomputers.

Nowadays the rapid development of computation equipment makes large computational tasks possible. Hamada et al.[31] used supercomputing equipment to investigate phase equilibria and interfacial tensions in confined cylindrical pores. A more general model was employed. In their work, 20×10^6 to 500×10^6 configurations were generated for equilibration, and 20×10^6

(35) Mecke, M.; Winkelmann, J.; Fischer, J. *J. Chem. Phys.* **1997**, *107*, 9264–9270.
(36) Yaws, C. L. *Physical Properties*; McGraw-Hill: New York, 1997.
(37) Kai, T.; Nomoto, H.; Deguch, M.; Takahashi, T. *J. Chem. Eng. Data* **1994**, *39*, 499–501.
(38) Reid, R. C.; Prausnitz, J. M.; Poling, B. E. *The Properties of Gases and Liquids*, 4th ed.; McGraw-Hill: New York, 1987.
(39) Puibasset, J. *J. Phys. Chem. B* **2005**, *109*, 8185–8194.
(40) Puibasset, J. *J. Chem. Phys.* **2007**, *127*, 154701.

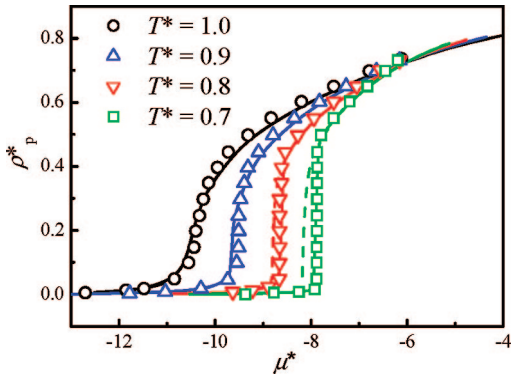

Figure 3. $\rho_p^*-\mu^*$ isotherms of Lennard-Jones fluids in hard cylindrical pores ($\varepsilon_w = 0$) with a diameter of $D = 5\sigma$. Symbols and solid lines represent the results from the GCMC simulations[27] and the present DFT, respectively. Dashed lines indicate hysteresis.

to 1.5×10^9 configurations were used for averaging. Compared to previous work,[39,41] the system was fairly large, and the length of the cylindrical cell (200σ) was long enough. This work provides very good simulation data to test the accuracy of the present DFT.

As for a real pore, the wall effect can be split into two parts: one is the purely geometric constraint expressed in hard walls as examined above, and the other is long-range interactions expressed in a nonuniform continuous potential field. The form of solid−fluid potential plays an important role in the structure of the density profile. To simplify the problem, a uniform potential averaged over the inner space of the real pore is used, as done by Hamada et al.[31] This simplification greatly underestimates nonuniformity of confined circumstance, especially the attraction near a solid wall, but in a narrow pore this effect may be less. Therefore, the interaction potential between Lennard-Jones fluid and a model cylindrical pore wall is expressed as

$$V^{ext}(r) = \begin{cases} \varepsilon_w, & r \le (D-\sigma)/2 \\ \infty, & \text{otherwise} \end{cases} \tag{24}$$

where ε_w is the well depth of the external potential, and D is the diameter of the cylindrical pore. The adsorption of the Lennard-Jones fluid (argon) in the cylindrical pore is represented as the average number density in the pore:

$$\rho_p = \frac{2}{R^2}\int_0^R \rho(r) r dr \tag{25}$$

where $R = D/2$ is the radius of the cylindrical pore. The pressure in the pore is obtained from the grand potential via

$$p_p = -\Omega/V \tag{26}$$

In Figure 3, the average density in the hard cylindrical pore ($D = 5\sigma$ and $\varepsilon_w = 0$) from the present DFT is compared with the GCMC simulation data as a function of chemical potential at different temperatures. The present DFT gives a good description of adsorption curves when compared with the GCMC simulations. We have seen from Figure 1b in the bulk fluid that the argon undergoes a gas−liquid first-order phase transition at $T^* = 1.0$, but this transition does not take place in a hard cylindrical pore with diameter $D = 5\sigma$ when $T^* \ge 0.9$, as predicted from both the present DFT and GCMC simulations due to the confinement of the cylindrical wall. Both the present DFT and GCMC simulations show that the argon in the pore is supercritical

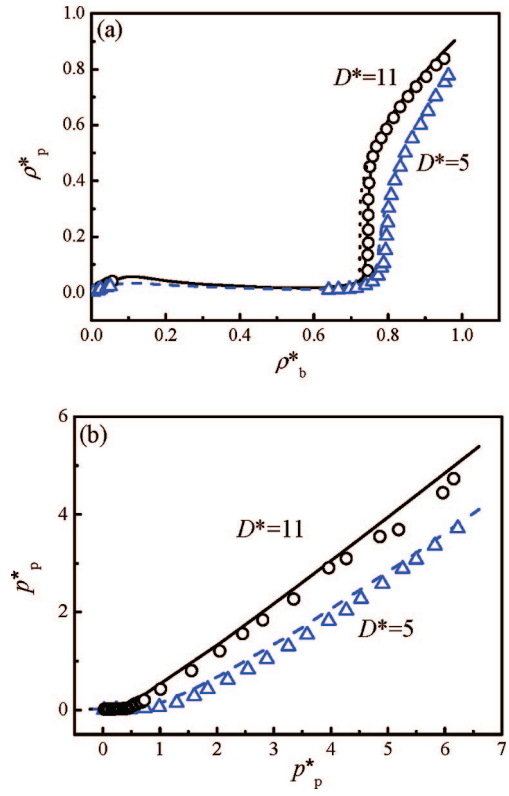

Figure 4. (a)$\rho_p^*-\rho_b^*$ and (b) $p_p^*-p_b^*$ isotherms of Lennard-Jones fluids in hard cylindrical pores ($\varepsilon_w = 0$) with different diameters ($D = 11$ and 5σ) at reduced temperature $T^* = 1.0$. Symbols and lines represent the results from the GCMC simulations[27] and the present DFT, respectively. Dashed lines and open triangles are for $D = 5\sigma$, solid lines and opened circles are for $D = 11\sigma$, and the dotted lines in panel "a" indicate hysteresis.

when $T^* \ge 0.9$, indicating that the critical temperature of the fluid in the pore is lower than that of bulk fluid. At a lower temperature $T^* = 0.7$, both the present DFT and GCMC simulation predict a first-order capillary condensation, and the only difference is that the gap between the adsorption/desorption branch of the simulations is nearly superimposed (not shown in Figure 3), but the one from the DFT is obvious. As the temperature is increased, the hysteresis loop narrows and disappears at the critical temperature in the pore.

The deviation of the critical temperature in the cylindrical pore between the present DFT and GCMC simulations may be attributed to dimension crossover, especially for narrow pores. When the pore radius becomes small, the fluid in the pore behaves like a one-dimensional fluid. In this case, if a DFT cannot reduce to the one-dimensional case, its performance will be bad in narrow pores. It seems that the present DFT does not behave well in narrow pores, and this results in a discrepancy between the theory and simulations at the phase transition for the Lennard-Jones fluid.

The average density and pressure in hard cylindrical pores of the Lennard-Jones fluid at $T^* = 1.0$ are plotted in Figure 4a,b, respectively. The cylindrical pores with diameters $D = 5$ and 11σ are considered. From Figure 4a one can see that $\rho_p^*-\rho_b^*$ isotherms calculated from the present DFT agree with the GCMC simulations very well. The present DFT nearly superimposes the GCMC simulations where the density increases abruptly. The horizontal part of $\rho_p^*-\rho_b^*$ curve for $D = 11\sigma$ represents the vapor−liquid phase transition in the bulk fluid, while the vertical part indicates the phase transition in the pore. There is no hysteresis loop found in the small pore with a diameter of 5σ, indicating

(41) Peterson, B. K.; Gubbins, K. E.; Heffeilfinger, G. S.; Marconi, U. M. B.; van Swol, F. *J. Chem. Phys.* **1988**, *88*, 6487–6500.

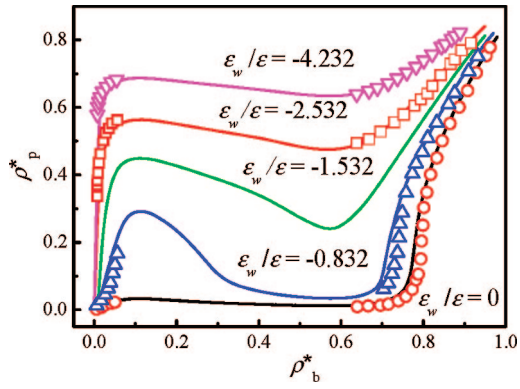

Figure 5. Comparison of predicted average density in the cylindrical pore ($D = 5\sigma$) with those from the GCMC simulations at reduced temperature $T^* = 1.0$ and different fluid−pore wall interactions. Symbols and lines represent the results from the GCMC simulations[31] and the present DFT, respectively.

that the fluid is supercritical at $T^* = 1.0$ in the pore, while, in the larger pore with a diameter of 11σ, a narrow hysteresis loop is found. At the same bulk density, the larger pore has a stronger adsorption due to the less repulsive effect of the hard cylindrical pore walls.

From Figure 4b one can see that the pressure in the pore predicted from the present DFT is slightly higher than those from the GCMC simulations. Figure 4b also shows that the pressure in the hard cylindrical pores is smaller than the corresponding bulk pressure. The pressure in the large pore is closer to the bulk pressure than that in the small pore in the case of hard cylindrical pores ($\varepsilon_w = 0$).

To investigate the effect of the fluid−pore wall attractive interaction, the average density and pressure in the pores with different wall parameters at $T^* = 1.0$ are presented in Figures 5 and 6, respectively. If the attractive potential is strong enough even at a very low bulk density, there is liquid-like dense fluid existing in the pore. As the attractive interaction becomes stronger, the wall−fluid attraction becomes dominant, resulting in average densities in the pore larger than the corresponding bulk ones. However, as the bulk density reaches the liquid branch, none of the potential can make $\rho_p^* = \rho_b^*$. The present DFT captures all these phenomena, and the predicted average densities in the pores are in good agreement with those from the molecular simulations.

Figure 6a shows that the pressures in the pore predicted from the present DFT agree fairly well with the GCMC simulations, and, as the wall attraction becomes stronger, the deviations between the present DFT and simulations are less appreciable. The stronger the pore wall attraction is, the higher the pressure in the pore. At high pressures, the magnitude of statistical error in the pressure is obvious for the molecular simulations, especially when the wall potential is strong and the density in the pore is high, but the present DFT can give a very smooth curve.

It is very interesting to examine the horizontal parts on the isotherms in Figure 5 and the crosses near $p_b^* = 0$ in Figure 6a. At the two end points of the horizontal parts with the same ρ_p^* corresponding to the vapor and liquid branches, the μ_b^* and p_p^* are same, while p_b^* is not necessarily the same. However, the cross points in Figure 6a have a same bulk pressure, indicating vapor−liquid phase equilibrium of the bulk fluid. To show this phenomenon clearly, we plotted the pressure in the pore at low bulk pressure region in Figure 6b. From this figure one can see that, for different attractive potentials, the pressure branch corresponding to vapor phase and the branch corresponding to liquid phase are intersected at the saturated bulk pressure. We

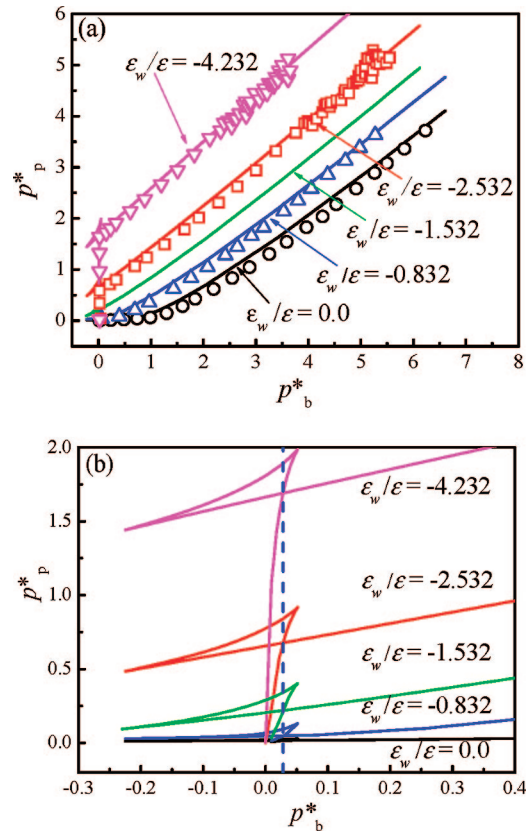

Figure 6. (a) Pressure in the cylindrical pore ($D = 5\sigma$) as a function of bulk pressure at reduced temperature $T^* = 1.0$ and different fluid−pore wall interactions, and (b) pressure in the pore at low bulk pressure region. The meaning of the symbols is the same as in Figure 5, except that the dashed vertical line in panel "b" indicates the bulk saturated pressure.

call it a stationary point that is always held in both attractive and repulsive pores.

3.3. Capillary Condensation of Nitrogen on MCM-41-Type Materials. The vapor in nanopores is able to condense into liquid-like dense fluid at gas pressure below the bulk saturated vapor pressure at some given temperatures. Since this transition occurs at a low pressure, it is difficult for the MF theory to get the results consistent with molecular simulations and experiments. In this work, the capillary condensation of nitrogen in cylindrical pores of MCM-41 type materials is modeled using the present DFT. To compare with the simulations, the Lennard-Jones parameters in the present DFT calculations are set to be the same as the GCMC simulations given in section 3.1, and the cutoff distance for fluid−fluid interactions is $r_c = 5.0\sigma$. This selection of the Lennard-Jones parameters is different from the literature,[7,20,22] where the parameters were obtained for nonlocal DFT by fitting experimental data.

The interaction between nitrogen and an MCM-41 cylindrical pore wall is expressed by the potential given by Tjatjopoulos:[42]

$$V^{ext}(r,R) = \pi^2\rho_s\varepsilon_{sf}\sigma_{sf}^2\left\{\frac{63}{32}\left[\frac{R-r}{\sigma_{sf}}\left(1+\frac{r}{R}\right)\right]^{-10}\cdot F\left[-\frac{9}{2},-\frac{9}{2};1;\left(\frac{r}{R}\right)^2\right] - 3\left[\frac{R-r}{\sigma_{sf}}\left(1+\frac{r}{R}\right)\right]^{-4}\cdot F\left[-\frac{3}{2},-\frac{3}{2};1;\left(\frac{r}{R}\right)^2\right]\right\} \quad (27)$$

where $R = D/2$ is the radial coordinate of the adsorption centers, ρ_s is the surface number density of the adsorption centers, and

(42) Tjatyopoulos, G. J.; Feke, D. L; Mann, J. A., Jr *J. Phys. Chem.* **1988**, *92*, 4006–4007.

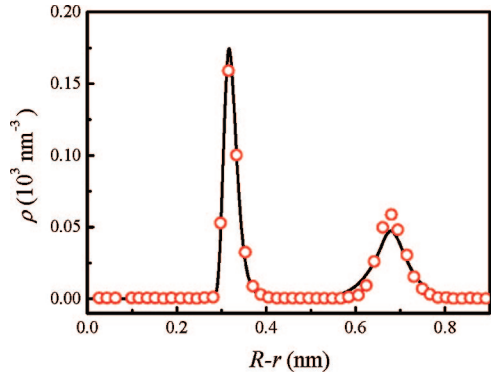

Figure 7. Comparison of predicted radical density profiles of nitrogen in a cylindrical pore with a diameter of $D = 5\sigma$ at 77.4 K and $p/p_0 = 0.014$. Open circles and the solid curve represent the results from the GCMC simulations[20] and the present DFT, respectively.

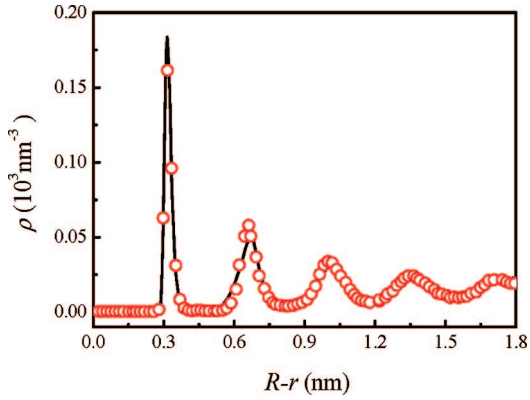

Figure 8. Comparison of predicted radical density profiles of nitrogen in a cylindrical pore with a diameter of $D = 10\sigma$ at 77.4 K and $p/p_0 = 0.38$. The meaning of the symbols is the same as in Figure 7.

$F[\alpha,\beta;\gamma;\delta]$ is the hypergeometric series. For nitrogen adsorption on MCM-41-type materials, we take the solid−fluid interaction parameters as $\rho_s = 15.3$ nm^{-2}, $\sigma_{sf} = 0.317$ nm, and $\varepsilon_{sf}/k_B = 147.3$ K, which were determined by Ravikovitch et al.[43] from the fit of experiemental data in the multilayer adsorption region.

Figures 7−9 depict comparisons of density profiles predicted from the present DFT with those from the GCMC simulations in MCM-41 cylindrical pores with diameters $D = 5$, 10, and 20σ, respectively. As can be seen from these figures, the density profiles from the present DFT match those from the simulations[20] very well. Under these conditions, the fluid in the pore is liquid-like, and the molecules arrange in annuli within the pore. For large pores (see Figure 9), there are particles existing in the center of the pore, while, when the diameter of the pore is reduced to a diameter of 5σ, only two annuli of molecules exist in the pore, and the density in the center is nearly zero. The first peak close to the wall has a similar high intensity in density for the pores with the three diameters, which suggests the wall−fluid attractive interaction is dominant. As can be seen by the nearly zero densities between the first two pronounced peaks, the particles in them can hardly move freely between these two annuli because the strong attractive force due to wall−particle interaction nearly fixes the first annulus of particles clinging to it. However, this kind of attractive force decays dramatically as the distance is increased, and the particles in the other adjacent peaks exchange more freely. In the center of the large cylindrical pores, where

(43) Ravikovitch, P. I.; Haller, G. L.; Neimark, A. V. *Adv. Colloid Interface Sci.* **1998**, *77*, 203–226.

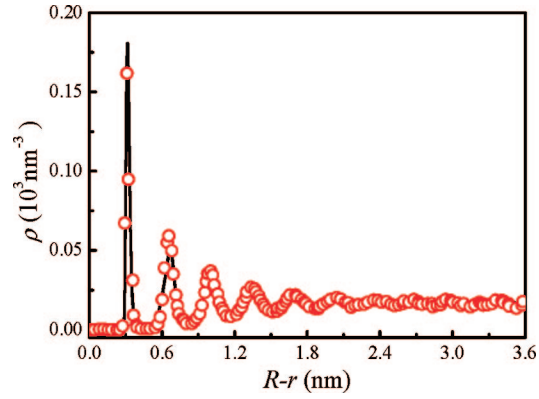

Figure 9. Comparison of predicted radical density profiles of nitrogen in a cylindrical pore with a diameter of $D = 20\sigma$ at 77.4 K and $p/p_0 = 0.822$. The meaning of the symbols is the same as in Figure 7.

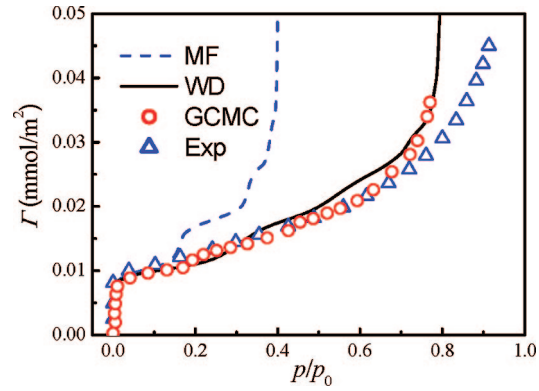

Figure 10. Adsorption isotherms of nitrogen on a silica cylindrical pore with a pore diameter $D = 24.9\sigma$ at 77.4 K. Open circles and triangles and dashed and solid lines represent the results from the GCMC simulations,[20] experimental standard adsorption on nonporous silica,[44] MF theory, and present DFT, respectively.

the molecules are far away from the solid walls, the solid−fluid potential affects fluid weakly, and the fluid in this area behaves like in the bulk case.

To investigate the adsorption of nitrogen on MCM-41 type materials, the adsorption of nitrogen was obtained by integrating density profiles,

$$\Gamma(\mu) = \frac{2}{D - \sigma_{ss}} \int_0^{D/2} \rho(r) r \mathrm{d}r \tag{28}$$

where $\sigma_{ss} = 0.276$ nm is the effective diameter for oxygen in silica. Since $\rho_b(\mu)$ is very small in this system, no calibration was included in the adsorption.

Figures 10−12 demonstrate adsorption isotherms of nitrogen on MCM-41-type materials with diameters $D = 24.9$, 20, and 14.9σ, respectively. In Figures 10−12, the transverse axis is p/p_0, where p and p_0 are the bulk pressure and bulk experimental saturated pressure (i.e., $p_0\sigma^3/\varepsilon = 3.585 \times 10^{-3}$) for nitrogen at 77.4 K, respectively. The adsorption and desorption isotherms calculated from the present DFT and GCMC simulations[20] agree well with each other. The adsorption is almost the same as the GCMC simulation data at single vapor or liquid phase. Only a slight overestimation occurs at vapor metastable states. Our method nearly reproduces the whole phase diagrams generated from the simulations. The adsorption isotherms from the MF approximation are similar in shape to those from the simulations, but an obvious deviation is observed. Since the bulk MF equation of state substantially underestimates the equilibrium pressure,

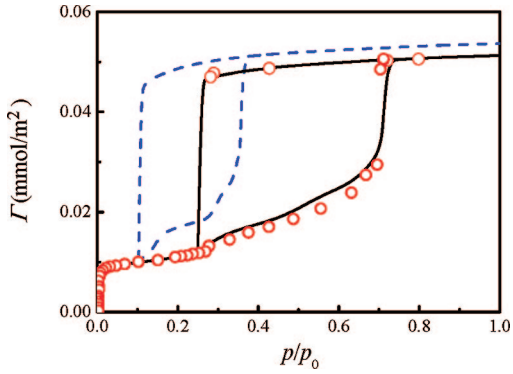

Figure 11. Adsorption isotherm of nitrogen in MCM-41 cylindrical pore with a pore diameter $D = 20\sigma$ at 77.4 K. Open circles and dashed and solid lines represent the results from the GCMC simulations,[20] MF theory, and present DFT, respectively.

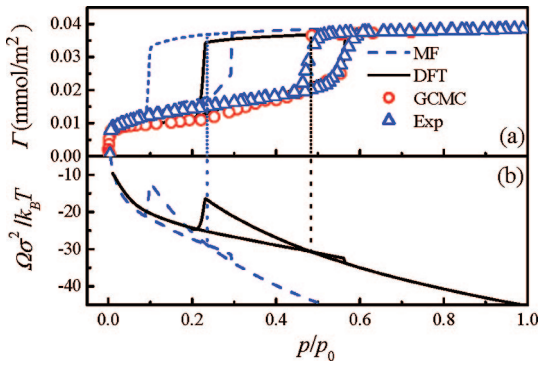

Figure 12. (a) Adsorption isotherms and (b) grand potentials of nitrogen on MCM-41 with a pore diameter $D = 14.9\sigma$ at 77.4 K. Open circles and triangles and dashed and solid lines represent the results from the GCMC simulations,[20] experiments,[45] MF theory, and present DFT, respectively.

the hysteresis loop moves to the lower pressure region in the density−pressure plane. It is a delicate problem to predict adsorption and desorption isotherms associated with pressure. Because of the large discrepancies in bulk properties, MF theory does not cope with such a delicate problem very well.

The grand potentials of the system are presented in Figure 12b, which demonstrates the DFT prediction capacity for the phase equilibrium of the nitrogen in the MCM-41 cylindrical pore. The present DFT predicts an excellent result for the vapor and liquid branches of adsorption. The hysteresis loop formed by the metastable adsorption and the equilibrium desorption branches from the present DFT are also in agreement with the experimental data,[44,45] which is the same as that of Ravikovitch et al.[20] The MF theory gives a similar saturated vapor and liquid density, but the saturated pressure predicted is much lower than the experimental data. Figures 10−12 show the potential application of the present DFT in the prediction of adsorption and phase equilibrium on MCM-41-type materials.

The effect of temperature on the adsorption of nitrogen on MCM-41-type materials with a large pore ($D = 20\sigma$) is illustrated in Figure 13. As the temperature is increased, the adsorption isotherm curve shifts toward high chemical potential region. At low temperature $T^* = 0.7$, there are two hysteresis loops in the isotherm curve. The left small hysteresis loop indicates a layer-transition at low pressure, and the right large hysteresis loop indicates a vapor−liquid capillary phase transition. As temperature

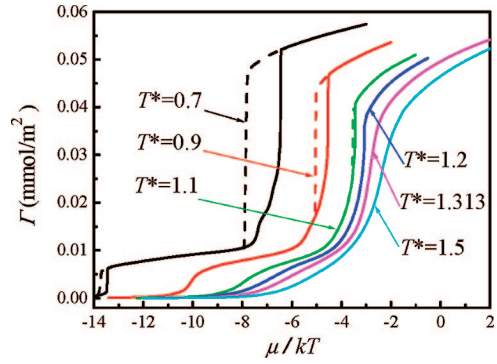

Figure 13. Predicted adsorption isotherms of nitrogen on MCM-41 with a pore diameter of $D = 20\sigma$ at different temperatures.

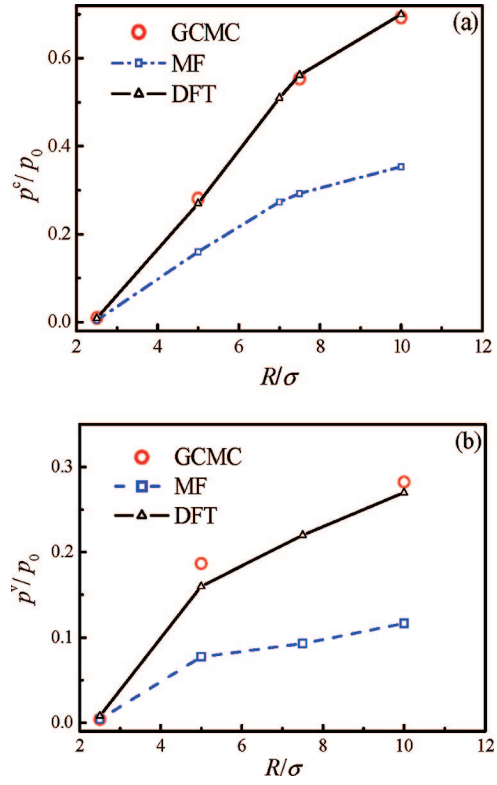

Figure 14. Dependence of (a) capillary condensation pressure and (b) capillary vaporization pressure on the pore size for nitrogen adsorption on MCM-41-type materials at reduced temperature $T^* = 77.4$ K. Open circles, triangles, and squares represent the results from GCMC simulations,[20] present DFT, and MF theory, respectively. Dashed and solid lines are guides to the eye.

is increased to $T^* = 0.9$, the left small hysteresis loop disappears, and the large hysteresis loop also disappears before temperature reaches the bulk critical temperature. This suggests that the vapor−liquid critical temperature of nitrogen in the MCM-41 cylindrical pore is lower than the corresponding bulk one.

Comparisons of predicted condensation and vaporization pressures with those from the GCMC simulations and MF theory at 77.4 K are demonstrated in Figure 14. Here the condensation and vaporization pressures, i.e., p^c and p^v, correspond to the right and left vertical lines of the hysteresis loop in the isotherms, respectively. It is shown in Figure 14 that both condensation and vaporization pressures of nitrogen increase as the radius of the MCM-41 pore is increased. The present DFT predicts accurate condensation pressure and slightly underestimates the vaporization pressure when compared with the GCMC simulations. In contrast, the MF theory substantially underestimates both

(44) DeBoer, J. H.; Linsen, B. G.; Osinga, T. J. *J. Catal.* **1965**, *4*, 643–649.
(45) Kruk, M.; Jaroniec, M.; Sayari, A. *Langmuir* **1997**, *13*, 6267–6273.

condensation and vaporization pressures.

4. Conclusions

Traditional MF approximation describing the attractive Lennard-Jones interaction in DFT can not reproduce accurate bulk properties when compared with molecular simulations and experiments. In this work, a DFT based on the MFMT and MBWR equation of state is presented. The attractive interaction is expressed as a functional of attractive weighted density. In this way, with the same set of Lennard-Jones parameters as in the molecular simulations, the present DFT is able to reproduce accurate bulk properties such as bulk chemical potential, equilibrium density, pressure and vapor−liquid surface tension.

The proposed DFT has been examined extensively using the recent published GCMC simulation data for the Lennard-Jones fluid (argon) confined in a model cylindrical pore. The average densities in the pore predicted from the present DFT are in good agreement with those from the simulations, and the pressures in the hard cylindrical pores are slightly overestimated. The effects of the fluid−pore wall interactions on average densities and pressures in the pores are also accurately described by the present DFT.

The present DFT has been applied to adsorption of nitrogen on MCM-41-type materials with different cylindrical pore diameters at 77.4 K. The density profiles calculated from the present DFT agree with those of the GCMC simulations very well. The adsorption isotherms predicted from the present DFT are in good agreement with the results from the GCMC simulations and experiments. In contrast, the hysteresis loop calculated from the MF theory moves toward the low pressure region because the MF equation of state predicts a low pressure of the bulk fluid. The present DFT predicts that the layer-transition takes place in the large MCM-41 pores at low temperature and pressure. The present DFT has potential in the prediction of adsorption and capillary condensation of simple gases on porous materials.

Acknowledgment. The authors greatly appreciate the financial support of the National Natural Science Foundation of China (No. 20676065 and No. 20736003), the Specialized Research Fund for the Doctoral Program of Higher Education (No. 20070003099), the National Basic Research Program of China (No. 2003CB615700), and the Program for New Century Excellent Talents in University (NCET) of China.

LA8024099